JOURNAL OF NANO- AND ELECTRONIC PHYSICS
Vol. 9 No 1, 01024(6pp) (2017)
ЖУРНАЛ НАНО- ТА ЕЛЕКТРОННОЇ ФІЗИКИ
Том 9 № 1, 01024(6cc) (2017)

DFT Study of Intrinsic and Induced *p*-type Conductivity of ZnO Material

F. Marcillo[1,2*], L. Villamagua[1,3,†], A. Stashans[1]

[1] *Grupo de Fisicoquímica de Materiales, Universidad Técnica Particular de Loja, Apartado 11-01-608, Loja, Ecuador*
[2] *Titulación de Ingeniería Química, Universidad Técnica Particular de Loja, Apartado 11-01-608, Loja, Ecuador*
[3] *Departamento de Química y Ciencias Exactas, Sección Fisicoquímica y Matemáticas, Universidad Técnica Particular de Loja, Apartado 11-01-608, Loja, Ecuador*

(Received 11 October 2016; revised manuscript received 19 October 2016; published online 20 February 2017)

Density functional theory and generalized gradient approximation including a Hubbard-like term was used in the present work to analyse *p*-type electrical conductivity as well as the switch of *n*-type → *p*-type conductivity in the ZnO materials. Results on atomic shifts indicate significance of Coulomb electrostatic interaction in finding the equilibrium state of the system. It is shown that the *p*-type electrical conductivity could be obtained by the N impurity doping into the *n*-type ZnO samples and also by considering zinc vacancy defect in otherwise pure ZnO crystal. Computed concentrations of free-carriers for different samples are compared to the available experimental data.

Keywords: Density functional theory, Electrical conductivity, *n*-type, *p*-type, ZnO material, Nitrogen doping, Zinc vacancy.

DOI: 10.21272/jnep.9(1).01024 PACS numbers: 72.S –, 61.72.U –, 71.15.Mb

1. INTRODUCTION

Wurtzite-type zinc oxide (ZnO) is considered to be a wide-bandgap (WBG) material due to its 3.4 eV direct forbidden energy gap [1]. The WBG characteristic is responsible for several properties of the material, including good transparency, high electron mobility [2] and room-temperature luminescence [3]. On the other hand, its large excitation energy (60 meV) endows the crystal with important properties such as lasing action based on exciton recombination and possibly polariton/exciton interaction even above the room temperature [4]. Thus, properties of the ZnO outnumber those of the other WBG materials (e.g., GaN, AlGaN, InGaN and SiC) [5], which points out ZnO as a potential candidate to replace indium in expensive indium-based devices [6].

However, despite many years of investigation, some properties of this material are still not well understood [7]. In the present work, in order to reduce the uncertainty, we have carried out the DFT + *U* analysis of some of its properties, with special focus on those ignited by intrinsic and extrinsic defects in its crystalline lattice. Firstly, the *n*-type crystal, hereafter known as ZnO + H and investigated in detail previously [8, 9], was doped with increasing concentrations of N atoms until the *p*-type conductivity was achieved. Secondly, the origin of intrinsic *p*-type conductivity in ZnO driven by a negatively charged Zn vacancy (V_{Zn}^{2-}) was also investigated. Our theoretical findings regarding *p*-type conductivity in ZnO as well as the switch from the *n*-type to *p*-type conductivity are backed up by some experimental studies. For example, the work of Barnes et al. [10] reports the evidence for *p*-type conductivity in N-doped ZnO. Likewise, Yu et al. [11] study the occurrence of ferromagnetism in N-doped ZnO. Ma et al. [12] suggest that Zn atom vacancy (V_{Zn}) could be responsible for the intrinsic *p*-type conductivity in ZnO.

This article is organized as follows. Section II details the computational method used throughout the investigation. Section III discusses the most remarkable results obtained in the study. Finally, section IV gives the article conclusions with a brief summary.

2. THEORETICAL APPROACH

2.1 Method and Models

Density functional theory (DFT) calculations were carried out by means of the Vienna *ab initio* simulation package (VASP) [13, 14]. The interaction between the core electrons and the valence electrons were treated through the projector augmented wave (PAW) pseudopotential method proposed by Bloch [15] and adapted later by Kresse and Joubert [16]. In order to account for the exchange-correlation potential, the generalized gradient approximation (GGA) according to the Perdew-Burke-Ernzerhof (PBE) scheme [17] was used. Moreover, the following valence configurations have been exploited here: $3d^{10}$ $4s^2$ for Zn, $2s^2$ $2p^4$ for O, $1s^1$ for H, and $2s^2$ $2p^3$ for N.

Any technique based on the DFT-GGA experiences considerable difficulties when trying to achieve a correct description of the energy gap (E_G) for materials containing *d*-electrons. One way to minimize this error is by including an intra-atomic interaction term for the strongly correlated electrons by an unrestricted Hartree-Fock approximation, resulting in the so-called DFT + *U* approximation. A value of 5.0 eV was used throughout this work as the correction factor *U* for the Zn 3*d* electrons. Accordingly, the computed E_G width was found to be equal to 3.1 eV. This value is very close to the corresponding experimentally available values

* fpmarcillo@utpl.edu.ec
† lmvillamagua@utpl.edu.ec

 © 2017 Sumy State University

(~ 3.4 eV) [1, 18].

The Brillouin zone of the 4-atom primitive unit cell (UC) was sampled by a k-point mesh of 9 × 9 × 5 according the Γ-centered Monkhorst-Pack (MP) grid scheme. In order to compute intrinsic point defects the UC was expanded twenty-seven times (3 × 3 × 3 extension), which resulted in a 108-atom supercell. The corresponding k-point mesh (3 × 3 × 2) for the supercell maintained the same separation of 0.04 Å-1 in the reciprocal space. A cut-off kinetic energy of 540 eV was used throughout the work.

Performed structure optimization for pure ZnO material led to the following lattice parameters: $a = 3.239$ Å, $c/a = 1.605$ and $u = 0.379$, which are in satisfactory agreement with the experimentally available data: $a = 3.25$ Å, $c/a = 1.602$ and $u = 0.375$ [1].

Density of states (DOS) play an important role when analyzing the type of conductivity acquired by the crystal, i.e., by localizing the position of Fermi level (E_F) within the corresponding DOS pattern. Furthermore, by multiplying the DOS pattern with the Fermi distribution function, $f(E)$, as shown in equation 1, the hole concentration (p_0) can be obtained.

$$p_0 = \int_{-\infty}^{E_C} g_V(E)[1 - f(E)]dE \quad (1)$$

A detailed explanation of this equation can be found in [19, 20].

Bader population analysis [21], alongside a careful analysis of the atomic positions allowed us to understand the nature of the atomic movements within the defective region of crystal.

3. RESULTS AND DISCUSSION

3.1 Induced *p*-type Conductivity in ZnO

Induced *p*-type conductivity was attained through increasing $N^{-3} \rightarrow O^{-2}$ anionic substitutions into an atomic arrangement already exhibiting *n*-type electrical conductivity (ZnO + H). The *n*-type conductive material has been studied by our group before and its features are described in detail elsewhere [9]. Here, we can briefly state that equilibrium configuration of the ZnO + H consists in H atom occupying precisely oxygen vacancy site. For such configuration the computed free-carrier density is found to be equal to 10^{20} e/cm^3, which is close to some experimental findings. ZnO + H system also exhibits magnetic moment being equal to 3.47 μ_B. The mechanism for obtaining the *p*-type conductivity in ZnO was suggested by Barnes et al. [10] in their experimental study of ZnO by means of the X-ray diffraction technique.

Modeling of N dopants have been done starting from 1.85 mol % concentration (one impurity doping) up to 7.41 mol % concentration (four impurity doping). As a result, it was determined that at 5.56 mol % (i.e., three N impurities) the switch *n*-to-*p* takes place. A number of different configurations have been considered for the 5.56 mol % concentration by changing relative distances between the N impurities and the H atom. Analysis of the system's total energies allowed us to identify four configurations (Table 1) having high chance to occur in the nature since these configurations have very close total energies. For the sake of brevity only lowest energy configuration, i.e., sample 1 (Fig. 1), will been analyzed; the behavior of the remaining three configurations stick closely to it.

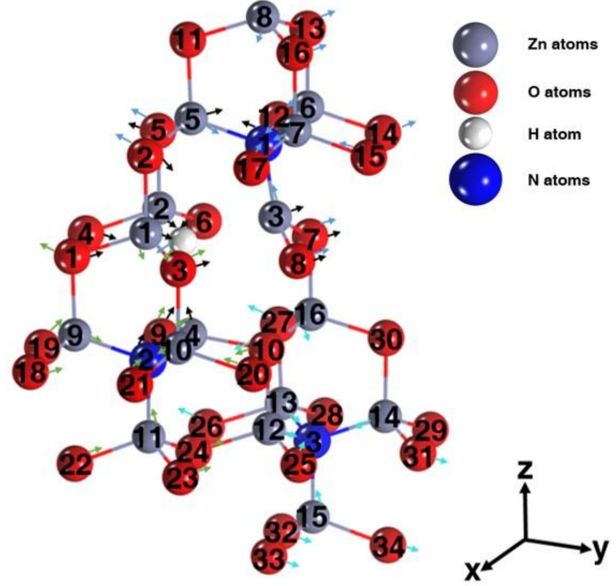

Fig. 1 – A schematic sketch showing the vicinity of N impurities and H atom situated within the oxygen vacancy site in the hexagonal ZnO material. Pointers indicate the direction of atomic movements due to the perturbation produced by the intrinsic and extrinsic defects

3.1.1 Analysis of the microstructure

Due to the N impurity-imposed perturbations atoms situated in the neighborhood of the defect suffer displacements, mostly driven by the Coulomb electrostatic interaction. Since atomic charge on N impurity is more negative than that of the replaced O atom, 0.07 e in average, stronger Coulombic attraction between the impurities and their surrounding Zn atoms occurs. That clearly explains the average defect-inward displacements of ~0.05 Å (Table 2) of the Zn atoms.

3.1.2 Electronic and magnetic properties

DOS pattern for the lowest energy configuration is shown in Fig. 2. It can be seen that the N dopants modify primarily the upper part of the VB. Thus, a strong contribution towards the *p*-type conductivity is due to the N 2p atomic orbitals (AOs). Zn 4*p*, Zn 3*d*, Zn 4*s* and O 2*p* AOs provide a noticeable contribution as well. Moreover, from the DOS picture one can notice the existence of unoccupied in-gap states in the beta spin electronic sub-system at ~ 0.31 eV and ~ 0.61 eV, respectively. Additionally, this configuration shows some band-gap shrinkage of ~ 1.17 eV with respect to ZnO + H system. The results on electronic features are in perfect agreement with the available experimental data [22-25].

It is important to mention that this configuration exhibits a magnetic moment being equal to 4.07 μ_B, which is larger as that computed for the ZnO + H system and being equal to 3.47 μ_B. There are some small

Table 1 – Summary of properties for samples 1 to 4: Energy difference (ΔE), which is given with respect to the most stable configuration (sample 1), band-gap (E_G) width, local magnetic moment induced by the H atom (m_H), local magnetic moment induced by the N atoms (m_N), total magnetic moment (m) and hole concentration (p_0)

Samples	N (mol%)	ΔE (eV)	Intrinsic defect	E_G (eV)	m_H (μ_B)	m_N (μ_B)	m (μ_B)	p_0 (holes/cm^3)
1	5.56	–	H_O	1.07	0.25	0.46	4.07	$1.291*10^{21}$
2		0.01		0.61	0.25	0.60	4.02	$6.314*10^{20}$
3		0.05		1.07	0.25	0.48	4.05	$1.467*10^{21}$
4		0.10		0.61	0.25	0.42	4.05	$1.150*10^{21}$

Table 2 – Atomic charges in the n-type material (q_1) containing Zn, O and H host atoms and in the p-type material (q_2) containing incorporated N impurities. Atomic displacements (Δr_1) for atoms situated in the vicinity of intrinsic and extrinsic defects with respect to the closest N impurity. Positive atomic displacements stand for outward movements. Numeration of the atoms corresponds to the one shown in Fig. 1

Extrinsic defects	Nearby atoms	q_1 (e)	q_2 (e)	Δr_1 (Å)
N (1) charge – 0.93 e	Zn (3)	0.75	0.71	– 0.06
	Zn (5)	0.88	0.83	– 0.06
	Zn (6)	0.85	0.83	– 0.05
	Zn (7)	0.85	0.85	– 0.05
	Zn (8)	0.86	0.86	– 0.04
	O (2)	– 0.86	– 0.82	0.02
	O (5)	– 0.85	– 0.84	0.02
	O (7)	– 0.84	– 0.86	0.06
	O (8)	– 0.84	– 0.88	0.06
	O (11)	– 0.88	– 0.85	–
	O (12)	– 0.85	– 0.84	– 0.01
	O (13)	– 0.85	– 0.85	0.01
	O (14)	– 0.83	– 0.84	0.01
	O (15)	– 0.83	– 0.83	– 0.02
	O (16)	– 0.85	– 0.86	0.02
	O (17)	– 0.84	– 0.85	– 0.02
	H_O	– 0.27	– 0.13	0.21
N (2) charge – 0.91 e	Zn (1)	0.75	0.68	– 0.05
	Zn (4)	0.77	0.73	– 0.02
	Zn (9)	0.84	0.84	– 0.04
	Zn (10)	0.84	0.85	– 0.05
	Zn (11)	0.83	0.83	– 0.09
	O (1)	– 0.84	– 0.85	0.03
	O (3)	– 0.84	– 0.86	0.02
	O (9)	– 0.85	– 0.86	0.01
	O (10)	– 0.84	– 0.84	– 0.02
	O (18)	– 0.85	– 0.83	– 0.02
	O (19)	– 0.84	– 0.84	0.01
	O (20)	– 0.84	– 0.84	– 0.01
	O (21)	– 0.85	– 0.86	– 0.02
	O (22)	– 0.84	– 0.82	0.01
	O (23)	– 0.84	– 0.83	0.02
	O (24)	– 0.87	– 0.83	0.05
	H_O	– 0.27	– 0.13	– 0.15
N (3) charge – 0.90 e	Zn (12)	0.83	0.83	– 0.02
	Zn (13)	0.84	0.84	– 0.04
	Zn (14)	0.84	0.83	– 0.03
	Zn (15)	0.84	0.82	– 0.05
	Zn (16)	0.84	0.87	– 0.03
	O (10)	– 0.84	– 0.84	0.02
	O (24)	– 0.87	– 0.83	–
	O (25)	– 0.84	– 0.84	– 0.01
	O (26)	– 0.84	– 0.83	0.01
	O (27)	– 0.84	– 0.84	0.03
	O (28)	– 0.84	– 0.84	–
	O (29)	– 0.84	– 0.82	–

	O (30)	– 0.85	– 0.83	–
	O (31)	– 0.85	– 0.84	0.01
	O (32)	– 0.84	– 0.83	0.01
	O (33)	– 0.87	– 0.85	0.03
	O (34)	– 0.84	– 0.83	0.02

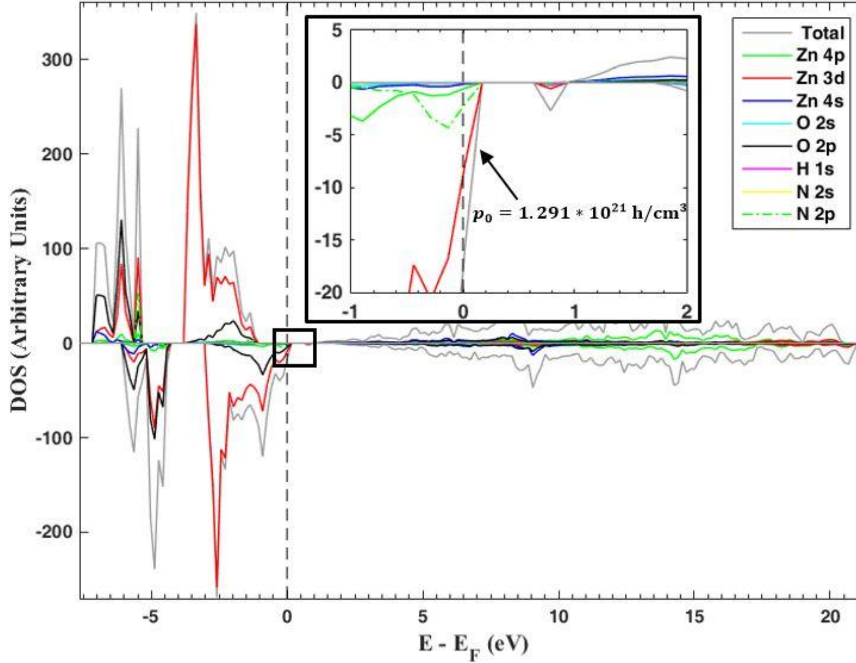

Fig. 2 – DFT + U computed total and partial DOS for the sample 1. Observed principal contribution in p-type conductivity (zoomed in the inset image) are due to the Zn 4p, Zn 3d, Zn 4s, O 2p and N 2p states. Vertical line denotes Fermi level (E_F)

changes of local magnetic moments on the host Zn, O and H atoms compared to their respective values in the ZnO + H system but the notable contribution towards the total magnetic moment of the supercell is due to N atoms, 0.46 μ_B.

3.2 Intrinsic *p*-type Conductivity in ZnO

Additionally, to the simulation of induced p-type conductivity we reproduced intrinsic p-type conductivity in the ZnO material. That was done by considering a Zn vacancy intrinsic point defect. Zn deficiency was modeled by removing one of the Zn host atoms from the central part of the 108-atom supercell as it is shown in Fig. 3.

3.2.1 Analysis of the microstructure

Table 3 displays atomic charges on Zn and O atoms. As one can observe, atomic charges for the crystal containing zinc vacancy in average changes by ~ 0.02 e/atom (increase) for zinc and ~ 0.09 e/atom (decrease) for oxygen, respectively. These changes are in direct correspondence to the displacements of the defect-neighboring atoms, which are also listed in Table 3 and depicted in Fig. 3b. Zn and O atoms displace themselves toward the V_{Zn} position by ~ 0.05 y ~ 0.09 Å, respectively. These movements are expected due to the natural trend of atoms to fill the empty space left by the atom removal.

The electron localization function (ELF) shown in Fig. 3a indicates the occurrence of V_{Zn}^{2-}, which shows no electron localization. The experimental evidence of the V_{Zn}^{2-} in ZnO, studied by different techniques, is widely explained elsewhere [26-30].

Table 3 – Bader charges on atoms for pure crystal, q_0, and ZnO:V_{Zn} system, q_1, as well as atomic displacements, Δr_2, for atoms situated in the vicinity of the intrinsic point defect. Positive atomic displacements stand for the outward movements. Numeration of the atoms corresponds to the one shown in Fig. 3

Nearby atoms	q_0 (e)	q_1 (e)	Δr_2 (Å)
O (1)	– 0.85	– 0.74	0.10
O (2)	– 0.85	– 0.74	0.10
O (3)	– 0.85	– 0.74	0.10
O (4)	– 0.85	– 0.73	0.09
O (5)	– 0.85	– 0.83	0.03
Zn (1)	0.85	0.86	– 0.06
Zn (2)	0.85	0.86	– 0.06
Zn (3)	0.85	0.87	– 0.06
Zn (4)	0.85	0.86	– 0.06
Zn (5)	0.85	0.86	– 0.06
Zn (6)	0.85	0.87	– 0.06
Zn (7)	0.85	0.86	– 0.06
Zn (8)	0.85	0.86	– 0.06
Zn (9)	0.84	0.87	– 0.06
Zn (10)	0.85	0.85	– 0.05
Zn (11)	0.85	0.85	– 0.05
Zn (12)	0.84	0.85	– 0.05

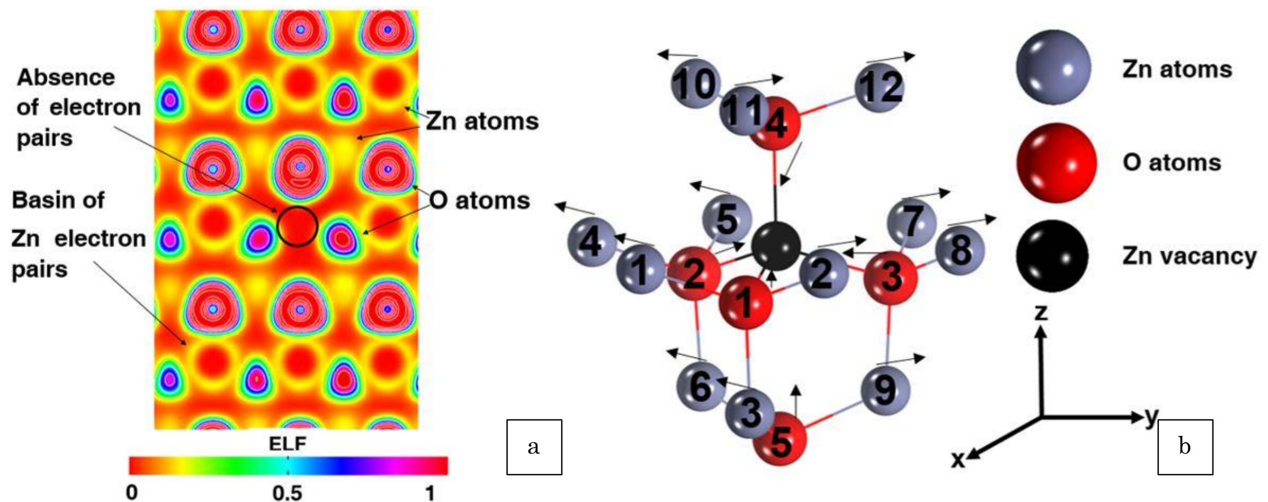

Fig. 3 – (a) Contour plot of the ELF for the ZnO:V_{Zn} material in the plane containing the V_{Zn}^{-2}, which perpendicular to the *z*-direction. Isoline small spheres represent O and Zn cores, respectively. The ELF scale is such that light (red/yellow online) means larger values of the ELF and dark (red online) means smaller value of the ELF. The black circle corresponds to the absence of Zn electron pair and is clearly seen. (b) A schematic figure of vicinity of the V_{Zn}^{-2} defect in the hexagonal ZnO crystal. The pointers indicate the direction of atomic movements due to the defect produced perturbation

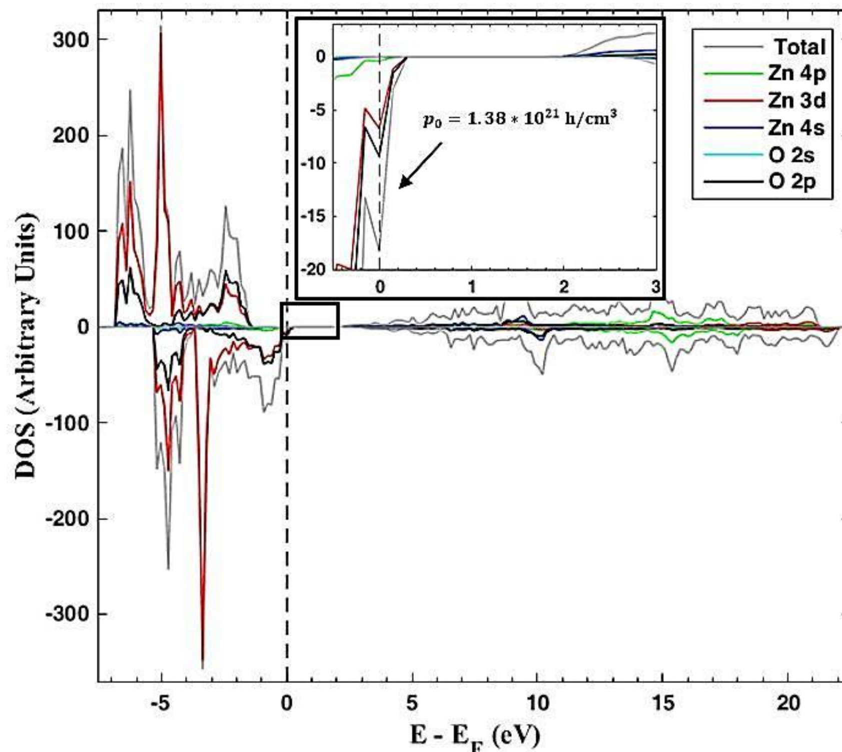

Fig. 4 – DFT + *U* computed total and partial DOS for the ZnO:V_{Zn} crystal, where the vertical line denotes the Fermi level (E_F). The zoomed part of DOS around the E_F (inset) indicates the contribution to the *p*-type conductivity and consists mainly of the Zn 4*p*, Zn 3*d* and O 2*p* states

4. CONCLUSIONS

Spin-polarized DFT + *U* calculations have been performed to investigate zinc oxide crystal and the *p*-type electrical conductivity. It is demonstrated that pure ZnO material can exhibit *p*-type conductivity if contains zinc vacancies. It is also shown that *n*-type ZnO material doped with N impurities switches from *n*-type to *p*-type if N impurity concentration reaches 5.56 mol %.

According to our results on crystal microstructure, Coulomb electrostatic interaction is mainly responsible for the atomic shifts in region containing intrinsic and extrinsic point defects. Nevertheless, tendency of atoms to fill the empty space left by the Zn atom removal also cannot be neglected.

Computed free-carrier densities for intrinsic and induced *p*-type conductivities are found to be equal to $1.38 \cdot 10^{21}$ holes/cm^3 and $1.29 \cdot 10^{21}$ holes/cm^3, respectively. These results are in good agreement with the avail-

able experimental data. It is also necessary to state that N impurity is found to be favorable to augment the magnetic moment of the ZnO + H samples. According to our computations, three N impurities contribute up to 0.46 μ_B towards the total magnetic moment of the supercell, which is equal to 4.07 μ_B. Undoped ZnO, ZnO:V_{Zn} system, is also found to display magnetism.

REFERENCES

1. H. Morkoç, Ü. Özgür, *Zinc oxide: fundamentals, materials and device technology* (John Wiley & Sons: 2008).
2. E.M. Fortunato, P.M. Barquinha, A.C. Pimentel, A.M. Gonçalves, A.J. Marques, R.F. Martins, L.M. Pereira, *Appl. Phys. Lett.* **85**, 2541 (2004).
3. M. Katsikini, *X-Ray Absorption Spectroscopy of Semiconductors* **190**, 49 (2015).
4. I.Y. Bu, *J. Alloy. Compd.* **509**, 2874 (2011).
5. A.L. Spetz, S. Nakagomi, H. Wingbrant, M. Andersson, A. Salomonsson, S. Roy, G. Wingqvist, I. Katardjiev, M. Eickhoff, K. Uvdal, *Mater. Manuf. Processes* **21**, 253 (2006).
6. B.S. Bae, Y.H. Hwang, J.S. Seo, G.M. Choi, *ECS Trans.* **50**, 101 (2013).
7. Q. Wang, Q. Sun, G. Chen, Y. Kawazoe, P. Jena, *Phys. Rev. B* **77**, 205411 (2008).
8. C.G. Van de Walle, *Phys. Rev. Lett.* **85**, 1012 (2000).
9. F. Marcillo, L. Villamagua, A. Stashans, *Int. J. Modern Phys. B,* submitted (2016).
10. T.M. Barnes, K. Olson, C.A. Wolden, *Appl. Phys. Lett.* **86**, 112112 (2005).
11. C.F. Yu, T.J. Lin, S.J. Sun, H. Chou, *J. Phys. D: Appl. Phys.* **40**, 6497 (2007).
12. Y. Ma, G. Du, S. Yang, Z. Li, B. Zhao, X. Yang, T. Yang, Y. Zhang, D. Liu, *J. Appl. Phys.* **95**, 6268 (2004).
13. A.J. Cohen, P. Mori-Sánchez, W. Yang, *Science* **321**, 792 (2008).
14. G. Kresse, J. Furthmüller, *Comput. Mater. Sci.* **6**, 15 (1996).
15. P.E. Blöchl, *Phys. Rev. B* **50**, 17953 (1994).
16. G. Kresse, D. Joubert, *Phys. Rev. B* **59**, 1758 (1999).
17. J.P. Perdew, K. Burke, M. Ernzerhof, *Phys. Rev. Lett.* **77**, 3865 (1996).
18. B.E. Sernelius, K.F. Berggren, Z.C. Jin, I. Hamberg, C. Granqvist, *Phys. Rev. B* **37**, 10244 (1988).
19. S. Prasad, H. Schumacher, A. Gopinath, *High-speed Electronics and Optoelectronics: Devices and Circuits* (Cambridge University Press: 2009).
20. P.M. Lee, Y.S. Liu, L. Villamagua, A. Stashans, M. Carini, C.Y. Liu, *J. Phys. Chem. C* **120**, 4211 (2016).
21. E. Sanville, S.D. Kenny, R. Smith, G. Henkelman, *J. Comput. Chem.* **28**, 899 (2007).
22. C. Persson, C. Platzer-Björkman, J. Malmström, T. Törndahl, M. Edoff, *Phys. Rev. Lett.* **97**, 146403 (2006).
23. X. Yang, A. Wolcott, G. Wang, A. Sobo, R.C. Fitzmorris, F. Qian, J.Z. Zhang, Y. Li, *Nano Lett.* **9**, 2331 (2009).
24. H. Nian, S.H. Hahn, K.K. Koo, E.W. Shin, E.J. Kim, *Mater. Lett.* **63**, 2246 (2009).
25. C. Shifu, Z. Wei, Z. Sujuan, L. Wei, *Chem. Eng. J.* **148**, 263 (2009).
26. D. Galland, A. Herve, *Phys. Lett. A* **33**, 1 (1970).
27. D. Galland, A. Herve, *Solid State Commun.* **14**, 953 (1974).
28. A. Taylor, G. Filipovich, G. Lindeberg, *Solid State Commun.* **8**, 1359 (1970).
29. W. Carlos, E. Glaser, D.C. Look, *Physica B: Condens. Matter.* **308**, 976 (2001).
30. L. Vlasenko, G. Watkins, *Phys. Rev. B* **72**, 035203 (2005).